Battery Management System with Lebesgue Sampling-Based Extended Kalman Filter

Wuzhao Yan, Bin Zhang, *Senior Member, IEEE*, Guangquang Zhao, *Member, IEEE*, Shijie Tang, Guangxing Niu, and Xiaofeng Wang *Member, IEEE*

Abstract—The estimation and prediction of State-of-Health (SOH) and State-of-Charge (SOC) of Lithium-ion batteries are two main functions of battery management system (BMS). In order to reduce the computation cost and enable deployment of BMS on low-cost hardware, Lebesgue sampling based extended Kalman filter (LS-EKF) is developed to estimate SOH and SOC. LS-EKF is able to eliminate unnecessary computations, especially when the states change slowly. In this paper, the SOH is firstly estimated and the remaining useful life (RUL) is predicted by LS-EKF. Then, the estimated SOH is used as the initial battery capacity for SOC estimation and prediction. The SOH and SOC estimation and prediction are calculated repeatedly in the whole battery service life. The proposed method is verified with the application to the capacity degradation of Lithium-ion battery. The results show that the LS-EKF based algorithm has a good performance in SOH and SOC estimation and prediction in terms of accuracy and computation cost.

Index Terms—Lebesgue sampling, State of health, state of charge, Lithium-ion battery, Extended Kalman filter.

I. Introduction

Batteries are safety critical components that provide power to system functions including command, control, communications, and intelligence [1]. It is important to improve the performance of battery management system (BMS) to make battery operation safe, reliable, and cost-efficient [2], [3]. BMS is designed to evaluate the instantaneous state-of-charge (SOC) in the battery and at the same time to monitor the slowly varying state-of-health (SOH).

SOC is an indicator that represents the available charge stored in the battery compared to the full capacity charge of the battery, given by a percentage of the current charge to the entire charge [4]. SOH describes the physical condition of a battery. Unlike SOC, there is no widely accepted definition of SOH. A general definition of SOH is that it quantifies the battery's ability to store energy and deliver specified performance compared to a fresh battery [5]. The total capacity

Manuscript received 09, 2017; revised 01, 2018 and 04, 2018; accepted 05, 2018.

Wuzhao Yan, Bin Zhang, Shijie Tang, Guangxing Niu, and Xiaofeng Wang are with the Department of Electrical Engineering, University of South Carolina, Columbia, SC.

(Bin Zhang: 803-777-8335; fax: 803-777-8049; e-mail: zhang-bin@cec.sc.edu).

Guangquan Zhao is with the Harbin Institution of Technology, Harbin,

of the battery is evaluated in terms of Amp-hours (Ah), which basically is a dimension of electric charge.

It's essential to accurately estimate the SOC and SOH in order to maximize and optimize the system operation. Knowing SOC also helps prevent overcharge and over discharge of batteries, which is vital for safe operation and long cycle life of lithium-ion batteries. However, both SOC and SOH are not directly observable, which requires estimation and prediction algorithms to provide real-time battery states [3], [6]–[9].

The easiest way to estimate SOH is based on current integration [10], [11]. Different estimation methods are also developed, including reduced state-space electrochemical models, artificial neural networks, and impedance spectroscopy [12]-[15]. These methods usually require a large computational cost, which makes them suitable for SOH estimation but not for SOC. The reason is that SOC estimation is often integrated with online real-time planning and control, which requires much faster and more accurate algorithms [4], [7], [16]. There are two main methods to estimate SOC. The first one is Coulomb counting method, which estimates SOC directly. However, it is sensitive to current error accumulation and requires accurate initial condition, which may not be available in many applications. The other method is open circuit voltage (OCV)-SOC conversion method, which uses the one-to-one mapping between SOC and OCV to estimate SOC. However, OCV cannot be measured directly in practical use since it needs a long rest time to achieve equilibrium in the battery before each measurement. Therefore, OCV estimation is often performed by using an equivalent circuit model (ECM) and the measured battery terminal voltage. With the OCV estimation, the SOC estimation can be obtained [17], [18].

Extended Kalman filter (EKF) is widely used in nonlinear system states estimation due to its simplicity [19]. EKF linearizes nonlinear system models, and calculates the mean and variance values of system states based on Bayesian theory. Traditionally, EKF is designed in Riemann sampling (RS), in which samples are taken in a periodic way and is denoted as RS-EKF. One major limitation of RS-EKF is its computational cost as the algorithm is executed every time when a measurement becomes available. To address this problem, Lebesgue sampling (LS) method is introduced with the advantage of reducing the computational cost by executing the algorithms "only when necessary" [20]. A SOH estimation and RUL prediction method was developed [21]. However, a BMS requires to monitor the two interconnected states, SOH and SOC, at the same time. To address this need, this research aims

to integrate SOC estimation with SOH estimation and RUL prediction in the framework of LS-EKF, which takes advantage of the merits of EKF and LS. In the proposed approach, SOH is estimated first, which is then used as the initial condition for SOC estimation. The SOC estimation is based on the online estimation of OCV and OCV-SOC conversion. Different from existing works, the proposed method estimates SOH and SOC algorithm simultaneously based on LS-EKF, which is verified with experimental results with better performance and much faster speed in estimation.

The paper is organized as follows: Section II provides the overview of the proposed LS-EKF. Section III illustrates the framework of the SOC and SOH estimation method. Section IV presents the verification of the algorithms by application to the degradation of SOH and variation of SOC of the Lithium ion batteries. Section V gives the concluding remarks with some future research topics.

II. THE PROPOSED LS-EKF METHOD

In the proposed method, SOH and SOC are estimated simultaneously. The value of SOC P_{SOC} can be obtained based on Coulomb counting method as:

$$P_{SOC} = \frac{Q_t}{Q_0} \times 100\% \tag{1}$$

where Q_t is the remaining capacity at current time instant and Q_0 is the total capacity. Assume the initial SOC value of the battery is P_{SOC_0} , Eq. (1) can be described as:

$$P_{SOC} = P_{SOC_0} - \frac{\int idt}{Q_0} \tag{2}$$

where i is the current, which is considered to be positive and negative for discharge and charge, respectively.

However, this Coulomb counting method has two limitations. One is that it starts from an initial SOC, which must be known and accurate. The other one is that the error originating from the sensor accuracy, current, and sampling frequency will accumulate over time and this method does not have the ability to recover from an inaccurate SOC estimation. To increase the accuracy and robustness of SOC estimation, a model-based SOC estimation method is developed [22], which utilizes OCV as an internal variable to estimates the SOC from a battery equivalent circuit model (ECM).

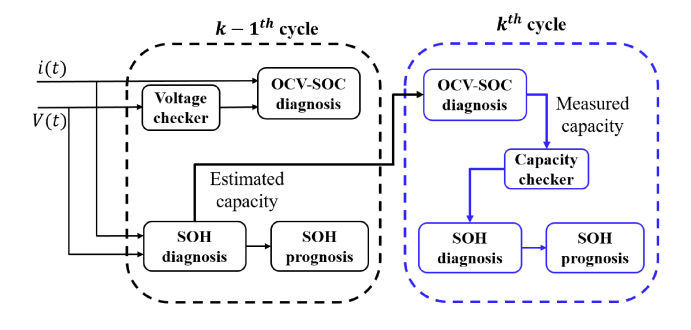


Fig. 1. Scheme of SOC and SOH diagnosis and prognosis

By utilizing this OCV-SOC conversion method, this paper develops a computational effective method to integrate the battery SOH and SOC diagnosis and prognosis in the framework of LS-EKF, as shown in Fig. 1, in which i(t) and V(t) are the measured current and voltage. In this figure, SOC is estimated based on OCV. As OCV measurement requires a long rest time to achieve equilibrium in the battery, it cannot be measured directly in practical use and needs to be estimated from battery model and terminal voltage. With OCV being estimated, the SOC estimation can be obtained since there exists a oneto-one OCV to SOC mapping [18]. The OCV-based SOC diagnosis is executed in each charge-discharge cycle with the SOH estimation from previous cycle as the initial condition to update the total capacity. At the end of each charge-discharge cycle, the battery SOH capacity is estimated and used to update the initial battery capacity for SOC estimation in the next cycle. This way, the SOC and SOH get estimated during the service life of the battery.

A. Lebesgue sampling method

A battery capacity degradation is used to illustrate the differences between RS and LS sampling methods. In Riemann sampling, samples are taken in a periodical manner, as shown in Fig. 2 (a). The battery SOH diagnosis and prognosis algorithm is executed at every charge-discharge cycle as long as a new measurement (based on Coulomb counting [23]) becomes available. This method ensures the tracking accuracy of the SOH state during the whole service life of the battery. However, it causes unnecessary computations when the battery SOH degradation is slow. Ideally, the number of SOH diagnosis and prognosis execution can be reduced when the battery SOH degradation is slow and increased when it is fast. To solve this problem, LS method is developed [20], [24], in which a number of Lebesgue states L_i , as shown by the horizontal lines in Fig. 2 (b), are defined on the battery capacity axis. The LS-based estimation algorithm is executed only when the measured battery capacity from Coulomb counting changes from one Lebesgue state to another, *i.e.*, an event happens. This philosophy significantly reduces the computation demands by eliminating unnecessary computation, especially when the battery capacity degradation speed is slow.

When prognosis is conducted, instead of calculating the battery SOH degradation at each future cycle (Fig. 2(a)), LS-based method will calculate the operation time for the battery SOH degrading to each predefined Lebesgue state (Fig. 2(b)). The calculated operation time reaching the Lebesgue state defined on the failure threshold will yield the time to failure, or RUL, directly.

Fig. 3 shows the difference between RS-based and LS-based prognosis. The prediction by RS-EKF (Fig. 3(a)) is conducted along the time axis, in which the state is predicted at each time instant until it reaches the failure threshold. The prediction horizon is the number of sampling points from current time instant to the time instant when the failure threshold is reached. For LS-EKF (Fig. 3(b)), the prediction is conducted along the state axis to achieve a time distribution at each Lebesgue state. The prediction horizon is the number of Lebesgue state from

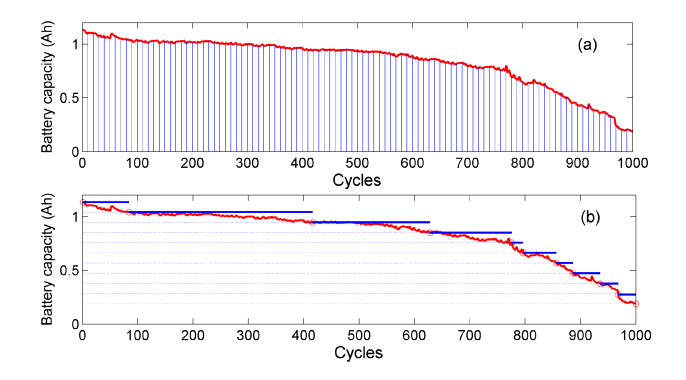


Fig. 2. The comparison between RS and LS. (a) RS with fixed time interval; (b) LS with fixed Lebesgue state length

current Lebesgue state to the Lebesgue state defined on the failure threshold. As we can see, the prediction horizon for LS-EKF is usually much smaller than that of RS-EKF. The worst case is that each measurement reaches a new Lebesgue state, the prediction horizon for LS-EKF is the same as that of RS-EKF.

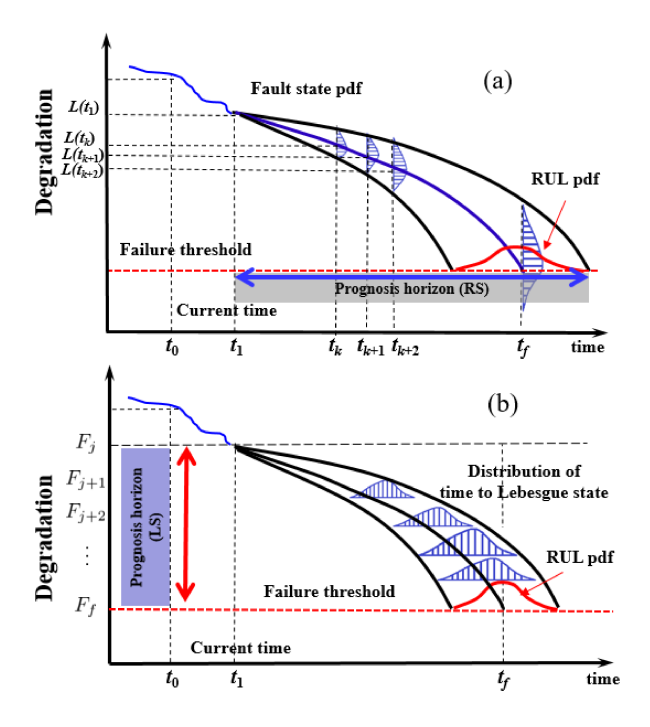


Fig. 3. The comparison between RS and LS prognosis. (a) RS prognosis; (b) LS prognosis.

With LS, the major difference of RS-EKF and LS-EKF are summarized as follows: In RS-EKF, the state estimation is conducted as long as a new measurement is available. The RUL prediction usually has a large prediction horizon, from the time instant when a battery degradation is detected at very early stage to a future time instant (given by charge-discharge cycle) that the battery degradation reaches the failure threshold. This long-term prediction not only requires a lot of computation resources, but also causes accumulation of uncertainties. For LS-EKF diagnosis, the state estimation is triggered only when an event happens. For LS-EKF prognosis, the RUL prediction horizon is defined on the state axis and

is described by the number of Lebesgue states. This gives us a straightforward method to conduct RUL prediction with the advantages of requiring little computation resources and resulting in small uncertainty accumulation.

However, the LS-based design is not intuitive compared to the traditional RS-based design. The LS-based prediction model in prognosis is not easy to be validated. As a result, LS-EKF leads to immediate challenges in design of models and algorithm, which will be addressed in the following sections.

B. LS-EKF for SOH diagnosis

EKF has been used for state estimation and RUL prediction in many systems, including batteries, [11] due to its low computational requirement. Traditional EKF algorithms are developed based on RS framework which is unfavorable from the computation-efficiency point of view in some cases, especially when the battery state degradation is slow. Lebesgue sampling method is developed [20] to reduce/increase the executions of algorithm when battery state degradation is slow/fast. In this section, the design of LS-EKF is explained with an example of diagnosis of battery SOH degradation.

In LS-EKF, the general form of SOH diagnosis model is given as [20]:

$$\hat{x}_{t_{k+1}} = f(\hat{x}_{t_k}, u_{t_k}, D_{t_k}) + \omega_{t_k} \tag{3}$$

where f is a nonlinear function, u_{t_k} is the input, which includes discharge current, temperature, and other environmental factors that affect battery capacity degradation, \hat{x}_{t_k} is the SOH state, ω_{t_k} is the Gaussian noise with covariance Q_{t_k} , which models the uncertainties, $D_{t_k} = L_{t_k,j+1} - L_{t_k,j}$ is the Lebesgue state length given by the distance between two adjacent Lebesgue states. Note that the Lebesgue states $L_{t_k,j}$ are adjusted according the battery degradation speed and, therefore, D_{t_k} is a nonlinear term. Here subscript t_k is the event stamp [20].

The observation model that describes the relationship between state x_{t_k} and measurements z_{t_k} is given by:

$$z_{t_k} = h(x_{t_k}) + v_{t_k} \tag{4}$$

where z_{t_k} is the measurement, which is battery capacity for SOH estimation and terminal voltage for SOC estimation, $h(\cdot)$ is the measurement function, v_{t_k} is a zero-mean Gaussian noises with covariance matrix R_{t_k} . Note that in our experiments, the battery is tested with an Arbin system, which provides capacity measurement via Coulomb counting. The measurement is used to compare with the predefined Lebesgue state $L_{t_k,i}$. If the measurement remains in the same Lebesgue state, the EKF algorithm will not be executed. Whenever the measurement reaches a new Lebesgue state, it triggers an event and the LS-EKF will be executed as follows.

The Jacobian of $f(\cdot)$ and $h(\cdot)$ are given by:

$$F_{t_{k-1}} = \frac{\partial f}{\partial x} \mid_{\hat{x}_{t_{k-1}|t_{k-1}}} \quad H_k = \frac{\partial h}{\partial x} \mid_{\hat{x}_{t_k|t_{k-1}}}$$
 (5)

Like other Bayesian methods, EKF algorithm includes two steps: the first step (prediction) is to propagate the state vector x into the next time step by using the state transition model;

the second step (update) is to correct the prediction from the first step by using the measurement z. The prediction step can be described as:

$$\hat{x}_{t_k|t_{k-1}} = f(\hat{x}_{t_{k-1}|t_{k-1}}, u_{t_{k-1}}, D_{t_{k-1}})
\Gamma_{t_k|t_{k-1}} = F_{t_{k-1}} \Gamma_{t_{k-1}|t_{k-1}} F_{t_{k-1}}^T + M_{t_{k-1}}$$
(6)

where $\Gamma_{t_k|t_{k-1}}$ and $M_{t_{k-1}}$ are the covariance matrices of the predicted state and the process noises.

The equations for the update step are expressed as:

$$K_{t_k} = \Gamma_{t_k|t_{k-1}} H_{t_k}^T (H_{t_k} \Gamma_{t_k|t_{k-1}} H_{t_k}^T + N_{t_k})^{-1}$$

$$\Gamma_{t_k|t_k} = (I - K_{t_k} H_{t_k}) \Gamma_{t_k|t_{k-1}}$$

$$\hat{x}_{t_k|t_k} = \hat{x}_{t_k|t_{k-1}} + K_{t_k} (z_{t_k} - h(\hat{x}_{t_k|t_{k-1}}))$$
(7)

where K_{t_k} is the near-optimal Kalman gain, N_{t_k} is the covariance matrix of the observation noises, $\Gamma_{t_k|t_k}$ is the updated covariance estimate, $\hat{x}_{t_k|t_k}$ is the updated state estimate, and I is the identity matrix. Note that the Jacobian needs to be calculated with the predicted state at each cycle.

C. LS-EKF for SOH prognosis

As described in Section II-A, the LS-EKF based prognosis predicts the operation time reaching each predefined Lebesgue state and this involves a model that describes the battery operation time as a function of battery capacity degradation. With this understanding, the prognosis model is given as:

$$\hat{t}_{k+1} = g(\hat{t}_k, \hat{x}_{t_k}, D_{t_k}) + \tau_{t_k} \tag{8}$$

where \hat{t}_k is the operation time distribution when the system state reaches the k-th Lebesgue state L_k , g is a nonlinear function, τ_{t_k} is a Gaussian noise term with covariance S_{t_k} .

Since prognosis involves long-term prediction without new measurement, there is no update step in the prognosis. Therefore, the prognosis will only conduct the prediction based on Eq. (8) and is implemented as:

$$\hat{t}_{k|k-1} = g_t(\hat{t}_{k-1|k-1}, \hat{x}_{t_{k-1}|t_{k-1}}, D_{t_k})
\Upsilon_{t_k|t_{k-1}} = G_{t_{k-1}} \Upsilon_{t_{k-1}|t_{k-1}} G_{t_{k-1}}^T + S_{t_{k-1}}$$
(9)

where $G_{t_{k-1}} = \frac{\partial g}{\partial t}$ is the Jacobin of Eq. (8), $\Upsilon_{t_k|t_{k-1}}$ and $S_{t_{k-1}}$ are the covariance matrices of the predicted time distribution and noise term, respectively.

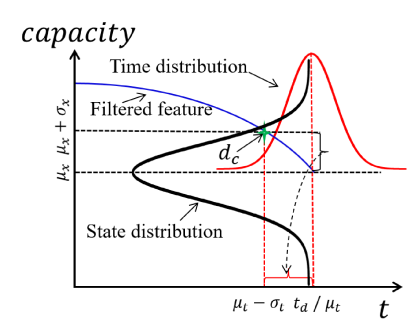


Fig. 4. Conversion from state distribution to time distribution

Note that the output of diagnosis at the time instant of the current event t_d is a state distribution, which cannot be used

in LS-based prognosis since prognosis requires an initial distribution of operation time. To obtain the time distribution on the current Lebesgue state, the state distribution is converted to a time distribution, as shown in Fig. 4. In the figure, the filtered SOH is the battery SOH estimation from LS-EKF. In this conversion, the time instant of the current event t_d is set to be the mean of the time distribution μ_t . The horizontal line $\mu_x + \sigma_x$ crosses the filtered battery SOH curve, marked as d_c in Fig. 4. The coordinates of the cross point $(\mu_t - \sigma_t, \mu_x + \sigma_x)$ indicate that state value $\mu_x + \sigma_x$ reaches the threshold at time instant $\mu_t - \sigma_t$. The time interval between t_d and d_c in Fig. 4 is considered to be the variance of the time distribution. By this means, the variance of state distribution σ_x is approximately converted to that of the time distribution σ_t . Here, μ_x , σ_x , μ_t , and σ_t are the mean and variance of the state estimation, the mean and variance of the time distribution, respectively.

D. LS-EKF for SOC diagnosis

This research conducts SOC estimation by using an OCV method [25], which is based on the measurement of the equilibrium OCV of the battery and a one-to-one mapping between OCV and SOC [18]. Since the equilibrium OCV cannot be measured for online use, this section develops a method to estimate OCV by integrating battery terminal voltage measurement and a second order ECM model as shown in Fig. 5 [26] in the framework of LS-EKF.

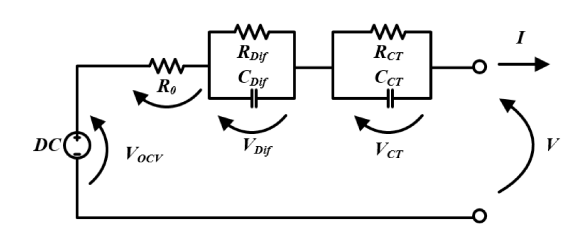


Fig. 5. Second order ECM for Lithium ion batteries [27].

Compared to the first-order ECM [28], this second order model better describes the battery dynamic characterized by hybrid pulse power characterization (HPPC) data. In this model, R_0 is the Ohmic resistance, i(t) is the discharge (positive) or charge (negative) current, V(t) is the measured voltage, V_{OCV} is the OCV of the battery, and V_{Dif} and V_{CT} are the voltage drop caused by the ion diffusion and the charge transfer, respectively. Note that R_{Dif} and C_{Dif} compose an RC circuit that describes the battery behavior caused by the ion diffusion. The second RC circuit formed by R_{CT} and C_{CT} represents the charge transfer process in the battery.

Based on this ECM model and the battery terminal voltage, the voltage drop in discrete time domain is given as:

$$\begin{cases} V_{CT}(t_k) = e^{-\frac{\Delta t}{\tau_{CT}}} \cdot V_{CT}(t_k - \Delta t) \\ + R_{CT} \cdot i(t_k - \Delta t) \cdot \left(1 - e^{-\frac{\Delta t}{\tau_{CT}}}\right) \\ V_{Dif}(t_k) = e^{-\frac{\Delta t}{\tau_{Dif}}} \cdot V_{Dif}(t_k - \Delta t) \\ + R_{Dif} \cdot i(t_k - \Delta t) \cdot \left(1 - e^{-\frac{\Delta t}{\tau_{Dif}}}\right) \end{cases}$$
(10)

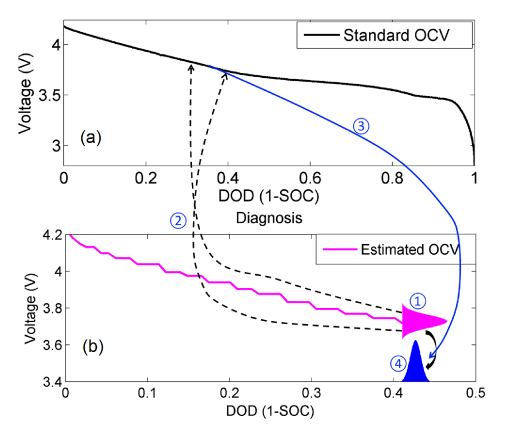
where Δt is the sampling period, and $\tau_{CT} = R_{CT}C_{CT}$ and $\tau_{Dif} = R_{Dif}C_{Dif}$ are the time constants of the two RC circuits in the ECM model. Note that this model is only calculated when the measured voltage reaches a new Lebesgue state in LS framework.

The relationship between the battery terminal voltage V and the open-circuit voltage V_{OCV} is given as:

$$V_{OCV}(t_k) = V(t_k) + V_{CT}(t_k) + V_{Dif}(t_k) + R_0 \cdot i(t_k)$$
 (11)

where R_0 is the battery internal ohmic resistance. The non-linearity of the model is in the OCV output calculated by Eq. (11), in which OCV is nonlinear with respect to $V_{CT}(t_k)$, $V_{Dif}(t_k)$, and SOC.

The parameters in Eqs. (10) and (11) can be identified by HPPC test [29] at the beginning of service life of the battery. To reduce the error from parameters in Eq. (11), the ECM parameters are updated with the degradation of SOH. For industrial applications, the influences from SOC, SOH, and temperature need to be considered in Eqs. (10) and (11).



D: calculate μ_{OCV} and CI_{OCV} ; D: calculate μ_{SOC} and CI_{SOC} ; D: build a Gaussian pdf for SOC based on μ_{SOC} and CI_{SOC} ;

Fig. 6. SOC pdf conversion converted from estimated OCV.

The LS-EKF SOC diagnosis is then implemented as follows: With the estimation of OCV, the SOC can be obtained from OCV-SOC look-up table [17], [18]. Since the OCV estimation from LS-EKF is given as a distribution, this involves the conversion from OCV distribution to SOC distribution as shown in Fig. 6. The V_{OCV} is estimated in LS-EKF by using measured voltage and Eq. (11). The estimated OCV-DOD (depth of discharge) curve, shown in Fig. 6 (b), is compared with the standard OCV-DOD curve shown in Fig. 6 (a) (obtained at the beginning of the battery service) to get the estimation of DOD and SOC is obtained by (1-DOD).

As the estimated OCV is a Gaussian distribution in LS-EKF, the estimation of SOC is also assumed to subject to a Gaussian distribution. First, mean (μ_{OCV}) and 95% confidence interval (CI) of OCV (CI_{OCV}) are calculated in LS-EKF. From these values, the corresponding μ_{SOC} and CI_{SOC} can be obtained on the standard OCV-SOC curve shown in Fig. 6(a). These values are then used to build a probability density function (pdf) of SOC, as shown in Fig. 6 (b).

III. EXPERIMENTAL VERIFICATION

In this section, the proposed method is demonstrated with an application to the SOC and SOH estimation of two Sony high drain 18650 Lithium-ion batteries with 2.25 Ah rated capacity. In this experiment, the capacity degradation is tested by Arbin BT2000 system under room temperature at a discharge current of 2.25 A. The battery capacity degradation is the decrease of the capacity with respect to charge-discharge cycles, as shown in Fig. 7. The failure threshold for SOH is set as 0.35 Ah and the batteries reach the threshold at the 928th and 822th cycles, respectively. From the experimental data, an empirical model is established and used in the diagnosis and prognosis. In real applications, the discharge current and its duration are recorded so that the capacity can be estimated by Coulomb counting [30]. The same idea is used in many researches [6], [221, [31], [32].

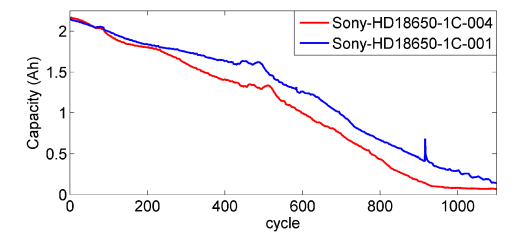


Fig. 7. The capacity degradation of two batteries.

The SOC data are collected in each charge-discharge cycle. Some examples of the collected data at different life stages of the battery are shown in Fig. 8. The horizon axis is the discharged capacity during one cycle, the vertical axis is the measured voltage during the test. The blue, red, and black curves show the capacity degradation trend in the initial state, middle stage, and late stage of battery service life.

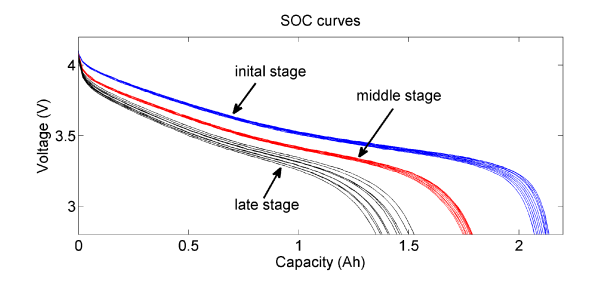


Fig. 8. V-SOC curves in different battery service life stages.

A. Parameter identification

The parameters of the second order ECM model need to be identified to estimate SOC based on Eqs. (10) and (11), which is conducted based on HPPC test [29] at the beginning of service life of the battery. The HPPC test consists of a series of discharge-charge pulse current at different SOC. Each discharge/charge pulse is 10 s with an amplitude of ± 1 C. A 0.05 C constant current is used to discharge the battery to the next SOC level to conduct another HPPC test.

The HPPC test results are shown in Fig. 9. With this data, the parameters are identified by least squares method

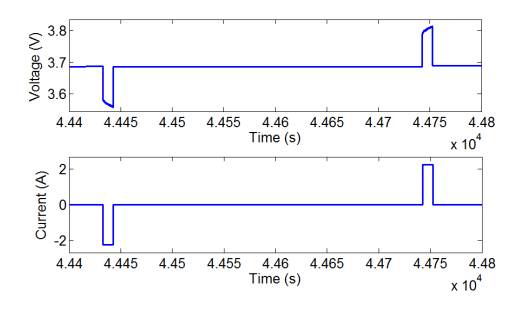


Fig. 9. HPPC data for a fresh battery at room temperature.

[32], which minimizes the sum of square error between the measured voltage and the voltage calculated by Eqs. (10) and (11). Since the dependence of parameters on SOC is negligible [28], the data collected from SOC=50% is chosen to identify the parameters. The results are shown in Eq. (12) and are used in OCV-SOC estimation.

$$\begin{cases} R_{CT} = 11.7m\Omega; \ \tau_{CT} = 7.1547s \\ R_{Dif} = 20.5m\Omega; \ \tau_{Dif} = 7.0459s; \\ R_0 = 44.7m\Omega \end{cases}$$
 (12)

B. Experimental results of LS-EKF

Figs. 7 and 8 show that the battery capacity (in the whole service life) and discharge capacity (in one discharge cycle) decrease with the increase of charge-discharge cycles and discharge time, respectively. To accommodate the influence of battery capacity degradation on SOC when SOH and SOC are integrated in BMS system, in the SOC estimation, the initial battery capacity Q_0 at each cycle must be updated based on the posterior pdf from the SOH estimation.

1) SOH estimation by LS-EKF: To implement LS-EKF for the battery capacity degradation, 40 uniformly distributed Lebesgue states are initially defined in the battery's full capacity of 2.25 Ah with consideration of our computation capability. With this setting, the diagnostic algorithm is executed only when the capacity degrades from one Lebesgue state to another. During the diagnosis process, the length of the Lebesgue states is optimally adjusted according to the battery SOH degradation speed. If it degrades faster, the next Lebesgue length will be decreased, otherwise, the next Lebesgue length will be increased [24].

In Lebesgue sampling framework, a diagnostic model is developed as [33], [34]:

$$C(t_{k+1}) = C(t_k) - p_d C(t_k)^{p_n} D(t_k) sgn(C(t_k) - C(t_{k-1})) + \omega(t_k)$$
(13)

where $sgn(\cdot)$ is a sign function and treated as positive or negative sign when calculating the Jacobian, C is the battery capacity, p_d and p_n are hyperparameters, which have values of 1.2 and 1.1, respectively, and the noise term $\omega(t_k)$ is required to be Gaussian. Note that this model is an explicit form of Eq. (3) for SOH diagnosis.

To illustrate the proposed algorithm, a Sony-HD18650-1C-004 battery is used as an example. Fig. 10 shows the diagnostic

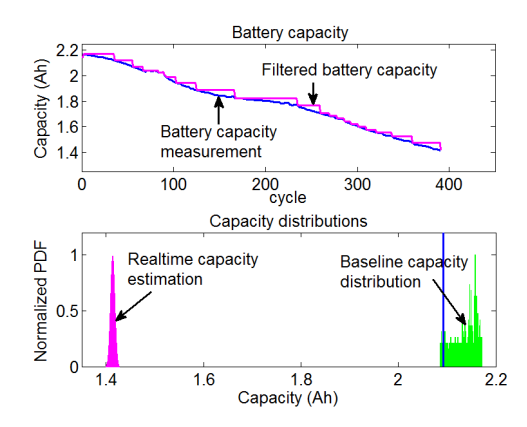


Fig. 10. LS-EKF diagnosis for battery at the 400th cycle.

results at the 400th cycle. The mean of capacity estimation is 1.414 and the 95% CI is [1.409, 1.419]. The upper sub-figure shows the comparison of capacity from Coulomb counting (blue) against the estimated mean value from diagnosis (magenta). The lower sub-figure shows the comparison of initial baseline pdf (green, created from the battery capacity at the beginning of service without degradation, which is the battery capacity values from Arbin system in the first 50 charge-discharge cycles) compared with the real-time estimated pdf at the 400th cycle. Note that the diagnostic algorithm is only executed 25 times in the past 400 cycles.

Prognosis is conducted by propagating the operating time distribution at each Lebesgue state, among which the one on the Lebesgue state that equals to the failure threshold is the RUL pdf. The prediction model is given as [33], [34]:

$$\hat{t}_{k+1} = \hat{t}_k + p_p \cdot C(t_k)^{p_t} \cdot D(t_k) \cdot exp\left(-\dot{C}(t_k)\right) + \tau(t_k)$$
 (14)

where p_p and p_t are hyperparameters with values of 975 and 0.45, respectively, and $\tau(t_k)$ is a Gaussian noise term. To use Eq. (14) for long-term prognosis, the initial distribution of the time distribution at the current Lebesgue state is converted from the current battery SOH distribution, as illustrated in Fig. 4.

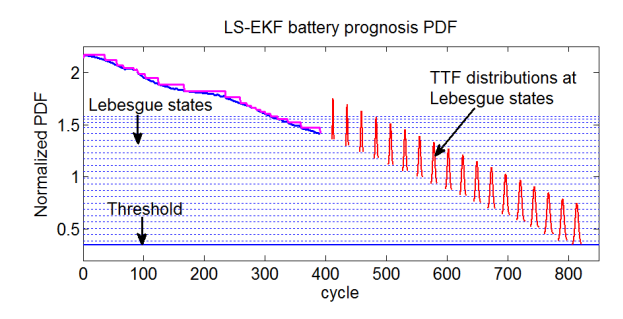


Fig. 11. LS-EKF prognosis for battery at the 400th cycle.

Fig. 11 shows the SOH prognostic results at the 400th cycle. The prediction horizon is 20 Lebesgue states. The pdf at the failure threshold is the predicted time to failure (TTF) for this battery with a mean value of 814.35 cycles and the RUL is 414.35 cycles. The 95% CI of the TTF distribution is [809.1 819.6], which indicates that the uncertainty accumulation is very small due to the small prediction horizon. Compared with

the ground truth TTF of 822, the difference between ground truth and the prediction is 7.65 cycles.

2) SOC estimation by LS-EKF: OCV estimation model in LS-EKF is given as follows by augmenting Eq. (11).

$$V_{OCV}(t_{k+1}) = V(t_k) - D(t_k) \cdot sgn(V(t_k) - V(t_{k-1})) + V_{Dif}(t_k) + V_{CT}(t_k) + R_0 \cdot i(t_k) + \omega_V(t_k)$$
(15)

where $\omega_V(t_k)$ is a Gaussian noise. Note that $sgn(\cdot)$ is a sign function same as in Eq. (13).

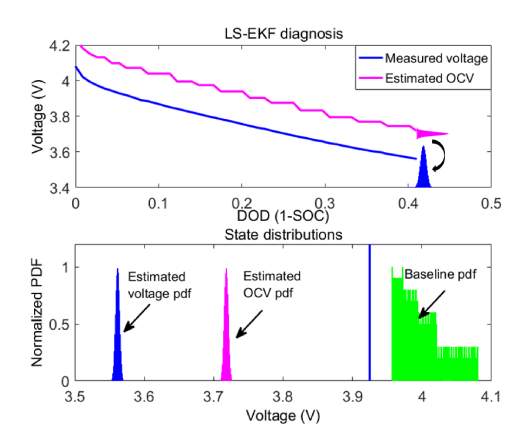


Fig. 12. Estimated OCV-SOC results by LS-EKF.

To run LS-EKF based SOC diagnosis, 40 Lebesgue states are defined on the voltage axis. The diagnosis algorithm is executed when an event happens (the voltage drops from one Lebesgue state to another one). Fig. 12 shows the results in the middle of a discharge cycle based on LS-EKF. The upper sub-figure is the comparison of the measured voltage from Arbin system against the OCV estimation by LS-EKF. The magenta curve is the OCV-SOC curve calculated from Eq. (15), in which V_{CT} and V_{Dif} are calculated by Eq. (10). The blue curve is the measured voltage. The bottom sub-figure shows the comparison of initial baseline pdf of OCV (green, constructed based on the first 50 measured voltage during the first charge-discharge cycle of the battery) compared with the real-time estimated OCV pdf (magenta). Note that the diagnostic algorithm is executed 18 times in the past 50 sampling points, which saves 64% computation.

The mean of OCV estimation is 3.72 V and the 95% CI is [3.7156, 3.7244] V. The corresponding CI of SOC can be found by mapping the standard OCV to SOC, which is obtained by Coulomb counting. CI_{DOD} and CI_{SOC} are [0.4115, 0.4251] and [0.5749, 0.5885], respectively.

C. Experimental results of RS-EKF

1) SOH estimation by RS-EKF: In RS-EKF, battery degradation model for diagnosis and prognosis is given as:

$$C(t+1) = C(t) - \gamma \cdot |p_1 \cdot (p_2 + p_3 \cdot t + p_4 \cdot t^2)|^{p_5} + \omega_C(t)$$
(16)

where $p = [1e^{-5}, 80, 0.08, -0.0008, 0.185]$, γ is a hyperparameter, $\omega_C(t)$ is a Gaussian noise, and t is the time index given by the charge-discharge cycles. The model is obtained by curve fitting and parameters are determined by identification.

Note that this is an explicit form of battery SOH degradation model in the RS framework.

Fig. 13 shows the diagnostic results at the 400th cycle of Sony-HD18650-1C-004 battery. The mean of capacity estimation is 1.4269 and the 95% CI is [1.4080, 1.4459]. The upper sub-figure is the comparison of the capacity from Arbin system against the capacity estimation from EKF. The bottom sub-figure shows the comparison of initial baseline pdf compared with the real-time estimated pdf (magenta) at the 400th cycle. Note that the diagnostic algorithm is executed 400 times in the past 400 cycles, *i.e.*, every time when a new measurement becomes available.

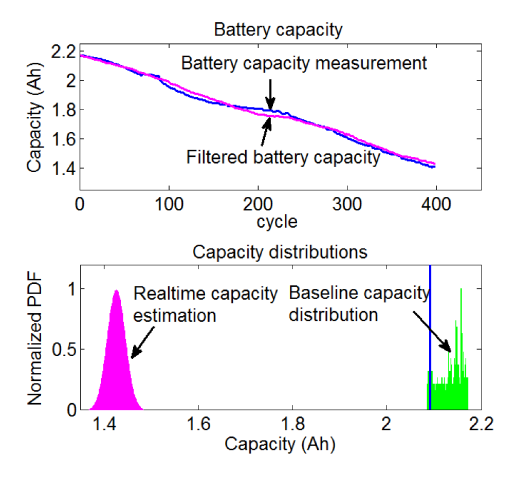


Fig. 13. RS-EKF SOH diagnosis for battery at the 400th cycle for Sony-HD18650-1C-004 battery.

With an estimation of the current battery capacity as the initial condition, the prognosis is executed to conduct the long-term prediction and estimation of RUL. Fig. 14 shows the expected value, upper and lower bounds of 95% CI of the battery capacity pdf at each future cycle.

The TTF distribution from prognosis is a Gaussian one with mean value of 806 cycles and the predicted RUL is 406 cycles. The prediction horizon is 444 cycles, which is very large compared to the prediction horizon of 20 Lebesgue states in LS-EKF. The standard deviation of the TTF distribution is 18.5 cycles. The distance between the prediction and ground truth is 16 cycles. The 95% CI of the RUL pdf is [769 843], which indicates that the uncertainty accumulated along the prediction horizon is very large.

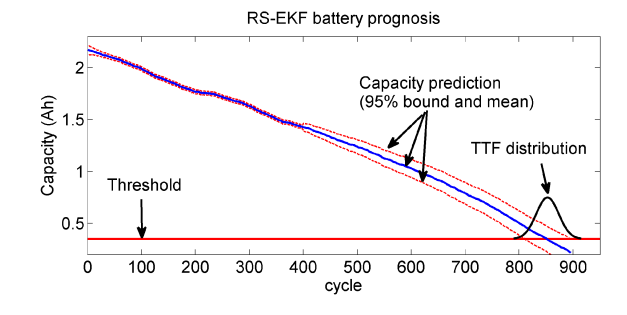


Fig. 14. RS-EKF SOH prognosis for battery at the 400th cycle.

2) SOC estimation by RS-EKF: OCV-SOC estimation results are achieved by RS-EKF based on Eqs. (10) and (11). Fig. 15 shows the results, at the same time as in Fig. 12. The upper sub-figure shows the comparison of measured voltage (blue) against the estimated mean value of OCV (magenta). The lower sub-figure shows the comparison of initial baseline pdf compared with the real-time estimated pdf. Note that the diagnostic algorithm is executed 50 times in the past 50 sampling data points, *i.e.*, every time when a new measurement becomes available.

The mean of OCV is 3.73 V and the 95% CI is [3.70, 3.76] V. With the same mapping method illustrated in Fig. 6, the results show that CI_{DOD} and CI_{SOC} are [0.3752, 0.4407] and [0.5593, 0.6248], respectively.

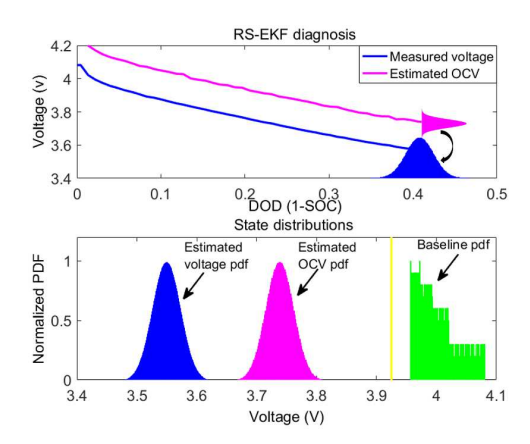


Fig. 15. Estimated OCV-SOC results by RS-EKF.

D. Comparison of RS-EKF and LS-EKF

1) Comparison of SOH estimation: Table I shows the comparison of diagnostic and prognostic results of RS-EKF and LS-EKF for SOH. The computation time at the 400th cycle for LS-EKF prognosis is only 6.64% of that of the RS-EKF prognosis.

TABLE I
COMPARISON OF SOH AT THE 400TH CYCLE

Diagnosis results	RS-EKF	LS-EKF
Capacity estimation	1.4269	1.414
Capacity 95% CI	[1.4080 1.4459]	[1.409 1.419]
Execution numbers	400 (100%)	25 (6.25%)
Prognosis results	RS-EKF	LS-EKF
True TTF	822	822
Estimate TTF	806	814.35
95% CI of TTF	[769 843]	[809.1 819.6]
Prognostic horizon	444	20
Computation time (s)	0.083668 (100%)	0.005553 (6.64%)

The results in Table I are a snapshot of diagnosis and prognosis at the 400th cycle. In order to compare SOH prognosis in the entire battery service life in terms of prediction accuracy, α - λ matrix is introduced [35], as shown in Fig. 16 with $\alpha=0.3$. It is clear from Fig. 16 that the mean of the predicted RUL for LS-EKF is as accurate as that of RS-EKF. However, the variance of predicted RUL of RS-EKF is much

smaller as shown in Table I, which is the natural benefit from Lebesgue sampling method: since the prediction horizon in LS-EKF is much smaller than that of LS-EKF, the uncertainty accumulation during the prediction process is much smaller. Based on these advantages, LS-EKF provides strong support for decision-making. More importantly, the LS-EKF required less calculation sources, which makes it promising for distributed diagnosis and prognosis algorithms to be deployed on hardware with limited computational sources.

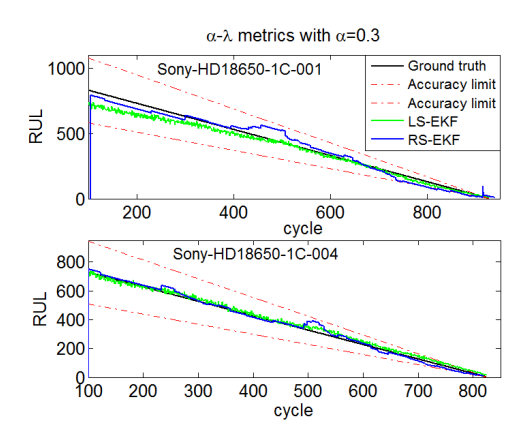


Fig. 16. Prediction accuracy comparison between RS-EKF and LS-EKF.

2) Comparison of SOC estimation: Table II shows the comparison of diagnosis of OCV from RS-EKF in Fig. 15 and LS-EKF in Fig. 12. Compared with RS-EKF diagnosis with 50 executions, the LS-EKF diagnosis only has 18 executions. The computation cost is only 36% of that of the RS-EKF.

TABLE II
COMPARISON OF OCV ESTIMATION

Diagnosis results	RS-EKF	LS-EKF
OCV estimation	3.7313	3.72
OCV 95% CI	[3.7031 3.7595]	[3.7156 3.7244]
Execution numbers	50 (100%)	18 (36%)

The standard OCV-SOC curve and the diagnosis results from RS-EKF and LS-EKF are shown in Fig. 17. The estimated OCV-SOC curves by RS-EKF (green) and LS-EKF (magenta) are both close to the standard OCV-SOC curve (black) compared with the measured V-SOC curve (blue). The root mean square (RMS) error of the estimated OCV-SOC curves from RS-EKF and LS-EKF are 0.05610 and 0.0601, respectively, which indicates an accurate OCV-SOC curve is achieved by LS-EKF method with less computation. Moreover, this result shows that the SOC equivalent circuit model used in this research is accurate enough. In the real applications, new HPPC tests can be conducted when the battery oeprating condition changes to accommodate the model uncertainty and improve the robustness of the proposed algorithm.

Note that it is difficult to provide fair comparison of RS-EKF and LS-EKF for SOH and SOC because they use different models and different algorithm designs. Therefore, the tables and figures in this section use some widely used criteria, such as mean, confidence interval, and computation time for comparison. The comparison shows that LS-EKF has much

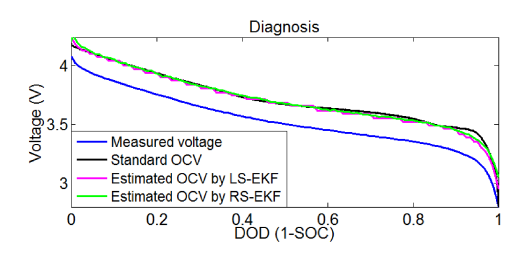


Fig. 17. The comparison between standard and estimated OCV-SOC curve by LS-EKF.

fast computation speed without sacrificing the accuracy and precision of SOH and SOC estimation.

IV. CONCLUSIONS

In order to reduce the computation of diagnosis and prognosis algorithms in BMS, a new method based on EKF is proposed in Lebesgue sampling framework. The proposed method integrates SOC and SOH diagnosis and prognosis in the framework of LS-EKF. In this research, the estimated SOH is first conducted and is used to update the initial value in SOC estimation to accommodate the limitations of existing works.

The proposed method is verified with a series of experiments of Lithium-ion battery SOH and SOC estimation with comparison against traditional RS-EKF approach. It is demonstrated that the proposed approach is able to reduce computation and provide reliable SOH and SOC estimation. This proposed approach combines the advantages of EKF and LS method, which results in low computation and small uncertainty accumulation. The future work will study batteries management under non-constant discharge rates, SOC increase in practical use by short-time recharge, such as regenerative braking in automotive industry, the influence of over-voltage and ECM parameters changes on SOC estimation.

REFERENCES

- B. Zhang, L. Tang, J. DeCastro, M. Roemer, and K. Goebel, "Autonomous vehicle battery state-of-charge prognostics enhanced misison planning," *International Journal of Prognostics and Health Management*, vol. 5, no. 2, pp. 1–12, 2014.
- [2] A. Sidhu, A. Izadian, and S. Anwar, "Adaptive nonlinear model-based fault diagnosis of Li-ion batteries," *IEEE Transactions on Industrial Electronics*, vol. 62, no. 2, pp. 1002–1011, 2015.
- [3] D. Liu, W. Xie, H. Liao, and Y. Peng, "An integrated probabilistic approach to lithium-ion battery remaining useful life estimation," *IEEE Transactions on Instrumentation and Measurement*, vol. 64, no. 3, pp. 660–670, 2015.
- [4] S. Piller, M. Perrin, and A. Jossen, "Methods for state-of-charge determination and their applications," *Journal of Power Sources*, vol. 96, no. 1, pp. 113–120, 2001.
- [5] B. Pattipati, K. Pattipati, J. P. Christopherson, S. M. Namburu, D. V. Prokhorov, and L. Qiao, "Automotive battery management systems." IEEE AUTOTESTCON, Salt Lake City, UT, 2008, pp. 581-586.
- [6] D. Liu, J. Pang, J. Zhou, Y. Peng, and M. Pecht, "Prognostics for state of health estimation of lithium-ion batteries based on combination gaussian process functional regression," *Microelectronics Reliability*, vol. 53, no. 6, pp. 832–839, 2013.
- [7] H. Sheng, J. Xiao, and P. Wang, "Lithium iron phosphate battery electric vehicle state-of-charge estimation based on evolutionary Gaussian mixture regression," *IEEE Transactions on Industrial Electronics*, vol. 64, no. 1, pp. 544–551, 2017.
- [8] R. Xiong, Y. Zhang, H. He, X. Zhou, and M. G. Pecht, "A double-scale, particle-filtering, energy state prediction algorithm for Lithium-ion batteries," *IEEE Transactions on Industrial Electronics*, 2017.

- [9] X. Hu, J. Jiang, D. Cao, and B. Egardt, "Battery health prognosis for electric vehicles using sample entropy and sparse Bayesian predictive modeling," *IEEE Transactions on Industrial Electronics*, vol. 63, no. 4, pp. 2645–2656, Apr. 2016.
- [10] Y. He, X. Liu, C. Zhang, and Z. Chen, "A new model for state-of-charge estimation for high-power li-ion batteries," *Applied Energy*, vol. 101, pp. 808–814, 2013.
- [11] S. C. L. da Costa, A. S. Araujo, and A. da Silva Carvalho, "Battery state of charge estimation using extended Kalman filter," in *Power Electronics, Electrical Drives, Automation and Motion (SPEEDAM)*, 2016 International Symposium on, pp. 1085–1092. IEEE, 2016.
- [12] J. D. Kozlowski, "Electrochemical cell prognostics using online impedance measurements and model-based data fusion techniques," in *Proceedings of Aerospace Conference*. 2003, vol. 7, pp. 3257–3270, 2003
- [13] O. Barbarisi, F. Vasca, and L. Glielmo, "State of charge Kalman filter estimator for automotive batteries," *Control Engineering Practice*, vol. 14, no. 3, pp. 267–275, 2006.
- [14] M. Charkhgard and M. Farrokhi, "State-of-charge estimation for lithiumion batteries using neural networks and EKF," *IEEE Transactions on Industrial Electronics*, vol. 57, no. 12, pp. 4178–4187, 2010.
- [15] D. Andre, C. Appel, T. Soczka-Guth, and D. U. Sauer, "Advanced mathematical methods of soc and soh estimation for lithium-ion batteries," *Journal of Power Sources*, vol. 224, pp. 20–27, 2013.
- [16] W.-Y. Chang, "The state of charge estimating methods for battery: A review," ISRN Applied Mathematics, vol. 2013, 2013.
- [17] M. A. Hannan, M. M. Hoque, S. E. Peng, and M. N. Uddin, "Lithium-ion battery charge equalization algorithm for electric vehicle applications," *IEEE Transactions on Industry Applications*, vol. 53, no. 3, pp. 2541– 2549, 2017.
- [18] B. Pattipati, B. Balasingam, G. Avvari, K. Pattipati, and Y. Bar-Shalom, "Open circuit voltage characterization of lithium-ion batteries," *Journal of Power Sources*, vol. 269, pp. 317–333, 2014.
- [19] P. Lall, R. Lowe, and K. Goebel, "Extended Kalman filter models and resistance spectroscopy for prognostication and health monitoring of leadfree electronics under vibration," in *Prognostics and Health Management (PHM)*, 2011 IEEE Conference on, pp. 1–12, Jun. 2011.
- [20] W. Yan, B. Zhang, X. Wang, W. Dou, and J. Wang, "Lebesgue-sampling-based diagnosis and prognosis for lithium-ion batteries," *IEEE Transactions on Industrial Electronics*, vol. 63, no. 3, pp. 1804–1812, 2016.
- [21] W. Yan and B. Zhang, "Extended Kalman filter development in Lebesgue sampling framework with an application to Li-ion battery diagnosis and prognosis," in *Third European Conference of the Prognostics and Health Management Society*. IEEE, 2016.
- [22] G. L. Plett, "Extended Kalman filtering for battery management systems of LiPB-based HEV battery packs: Part 3. state and parameter estimation," *Journal of Power Sources*, vol. 134, no. 2, pp. 277–292, 2004.
- [23] M. Gao, Y. Liu, and Z. He, "Battery state of charge online estimation based on particle filter," in *Image and Signal Processing (CISP)*, 2011 4th International Congress on, vol. 4, pp. 2233–2236. IEEE, 2011.
- [24] W. Yan, B. Zhang, W. Dou, D. Liu, and Y. Peng, "Low-cost adaptive Lebesgue sampling particle filtering approach for real-time li-ion battery diagnosis and prognosis," *IEEE Transactions on Automation Science and Engineering*, vol. PP, no. 99, pp. 1–11, 2017.
- [25] M. Coleman, C. K. Lee, C. Zhu, and W. G. Hurley, "State-of-charge determination from emf voltage estimation: Using impedance, terminal voltage, and current for lead-acid and lithium-ion batteries," *IEEE Transactions on Industrial Electronics*, vol. 54, no. 5, pp. 2550–2557, 2007
- [26] P. Moss, G. Au, E. Plichta, and J. Zheng, "An electrical circuit for modeling the dynamic response of Li-ion polymer batteries," *Journal of The Electrochemical Society*, vol. 155, no. 12, pp. A986–A994, 2008.
- [27] M. Chen and G. A. Rincon-Mora, "Accurate electrical battery model capable of predicting runtime and IV performance," *IEEE Transactions* on *Energy Conversion*, vol. 21, no. 2, pp. 504–511, 2006.
- [28] X. Tang, X. Mao, J. Lin, and B. Koch, "Li-ion battery parameter estimation for state of charge," in *American Control Conference (ACC)*, 2011, pp. 941–946. IEEE, 2011.
- [29] K. Amine, C. Chen, J. Liu, M. Hammond, A. Jansen, D. Dees, I. Bloom, D. Vissers, and G. Henriksen, "Factors responsible for impedance rise in high power Lithium ion batteries," *Journal of Power Sources*, vol. 97, pp. 684–687, 2001.
- [30] K. Ng, C. Moo, Y. Chen, and Y. Hsieh, "Enhanced Coulomb counting method for estimating state-of-charge and state-of-health of lithium-ion batteries," *Applied energy*, vol. 86, pp. 1506–1511, 2009.

- [31] W. He, N. Williard, M. Osterman, and M. Pecht, "Prognostics of lithiumion batteries based on Dempster-Shafer theory and the Bayesian Monte Carlo method," *Journal of Power Sources*, vol. 196, no. 23, pp. 10314– 10321, 2011.
- [32] C. Taborelli and S. Onori, "State of charge estimation using extended Kalman filters for battery management system," in *Electric Vehicle Conference (IEVC)*, 2014 IEEE International, pp. 1–8. IEEE, 2014.
- [33] X. Wang and B. Zhang, "Real-time Lebesgue-sampled model for continuous-time nonlinear systems," in *Decision and Control (CDC)*, 2014 IEEE 53rd Annual Conference on, DOI 10.1109/CDC.2014.7040070, pp. 4367–4372, Dec. 2014.
- [34] X. Wang and B. Zhang, "Lebesgue approximation model of continuoustime nonlinear dynamic systems," *Automatica*, vol. 64, pp. 234–239, 2016.
- [35] A. Saxena, J. Celaya, B. Saha, S. Saha, and K. Goebel, "Metrics for offline evaluation of prognostic performance," *International Journal of Prognostics and Health Management*, vol. 1, no. 1, pp. 4–23, 2010.



Wuzhao Yan received his B.A and Ph.D in Physics from University of Science and Technology of China, Hefei, China, in 2005 and 2010, respectively. He is currently working towards the Ph.D. degree in electrical engineering, University of South Carolina, Columbia, SC, USA.

From 2010 to 2013, he worked in Amperex Technology Limited, Dongguan, China, for 3 years. His research focuses on the algorithms of diagnosis and prognosis for lithium ion batteries and mechanical systems.



Bin Zhang (SM'08) received the B.E. and M.E. degrees in Mechanical Engineering from Nanjing University of Science and Technology, Nanjing, China, in 1993 and 1999, respectively, and the Ph.D. degree from Nanyang Technological University, Singapore, in 2007.

He is currently with the Department of Electrical Engineering, University of South Carolina, Columbia, SC, USA. Before that, he was with R&D, General Motors, Detroit, MI,

USA; with Impact Technologies, Rochester, NY, USA; and with the Georgia Institute of Technology, Atlanta, GA, USA. His current research interests include prognostics and health management, intelligent systems and controls, and their applications to various engineering systems.



Guangquan Zhao (M'14) received the B.E., M.E., and Ph.D. degrees in Instrumentation Science and Technology from Harbin Institute of Technology, Harbin, China, in 2000, 2002 and 2007, respectively.

He joined the Department of Automatic Test and Control, Harbin Institute of Technology in 2002, where he has developed his research activity. He is currently an Associate Professor at this university. His current research interests include deep learning, data-driven fault

diagnosis and prognosis, and their applications to various engineering systems.

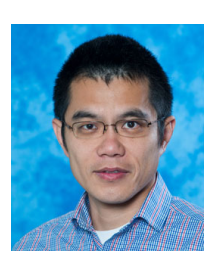


Shijie Tang received the B.E. degree in Electrical Engineering from Yanshan University, Qinhuangdao, China, in 2016. He is currently pursuing the Ph.D. degree in Electrical Engineering at University of South Carolina, Columbia, South Carolina, US.

His current research interests are Fault Diagnosis, Prognostic and Health Management, Machine Learning and Control Theory.



Guangxing Niu received his B.A degree in electrical engineering from North University of China, Taiyuan, China, in 2014,and received his M.S.E. degree in electrical engineering from Harbin Institute of Technology, Harbin, China, in 2016. He is currently working towards the Ph.D degree in electrical engineering, University of South Carolina, SC, USA. His research focus on the data-driven based algorithms of diagnosis and prognosis for lithium ion batteries and mechanical systems.



Xiaofeng Wang (S'06-M'09) received BS and MS degree in mathematics from East China Normal University in 2000 and 2003, respectively, and obtained his PhD degree in electrical engineering from the University of Notre Dame in 2009. After working as postdoctoral research associate in the Department of Mechanical Science and Engineering at the University of Illinois at Urbana-Champaign, he joined the Department of Electrical Engineering as assistant professor

at the University of South Carolina, Columbia, in 2012. His research interests include networked control systems, real-time systems, event-based control, robust adaptive control, distributed systems, and optimization.